Eur Biophys J (2009) 38:923–939
DOI 10.1007/s00249-009-0473-6

ORIGINAL PAPER

Human erythrocyte flickering: temperature, ATP concentration, water transport, and cell aging, plus a computer simulation

David Szekely · Tsz Wai Yau · Philip W. Kuchel

Received: 10 March 2009 / Revised: 26 April 2009 / Accepted: 29 April 2009 / Published online: 31 May 2009

Abstract Images of human erythrocytes from a healthy donor were recorded under differential interference contrast (DIC) microscopy; they were acquired rapidly (~336 Hz) and the intensity of the centermost pixel of each cell was recorded for ~60 s (20,000 values). Various techniques were used to analyze the data, including detrended fluctuation analysis (DFA) and multiscale entropy (MSE); however, power spectrum analysis was deemed the most appropriate for metrifying and comparing results. This analysis was used to compare cells from young and old populations, and after perturbing normal conditions, with changes in temperature, adenosine triphosphate (ATP) concentration (using NaF, an inhibitor of glycolysis, and α-toxin, a pore-forming molecule used to permeabilize red cells to ATP), and water transport rates [using glycerol, and *p*-chloromercuriphenylsulfonic acid (pCMBS) to inhibit aquaporins, AQPs]. There were measurable differences in the membrane fluctuation characteristics in populations of young and old cells, but there was no significant change in the flickering time series on changing the temperature of an individual cell, by depleting it of ATP, or by competing with the minor water exchange pathway via AQP3 using glycerol. However, pCMBS, which inhibits AQP1, the major water exchange pathway, inhibited flickering in all cells, and yet it was restored by the membrane intercalating species dibutyl phthalate (DBP). We developed a computer model to simulate acquired displacement spectral time courses and to evaluate various methods of data analysis, and showed how the flexibility of the membrane, as defined in the model, affects the flickering time course.

Keywords ATP concentration · Flickering · DIC microscopy · High-speed imaging · Human red blood cells · In vivo aging · Membrane undulations · Numerical simulation · Spectrin cytoskeleton · Water transport

Abbreviations

AQP	Aquaporin
ATP	Adenosine triphosphate
DBP	Dibutyl phthalate
DEP	Diethyl phthalate
DFA	Detrended fluctuation analysis
DIC	Differential interference contrast
MSE	Multiscale entropy
NMR	Nuclear magnetic resonance
pCMBS	*p*-Chloromercuriphenylsulfonic acid
RBC	Red blood cell
RF	Radio frequency
t	Time
TEP	Triethyl phosphate

Introduction

Rapid undulatory motion (flickering) in human erythrocyte (RBC) membranes was first described in 1890 (Browicz 1890) and these observations were later confirmed in 1901 (Cabot 1901). With the advent of phase-contrast microscopy nearly 50 years later (Pulvertaft 1949) redescribed the phenomenon. Flickering has since been revisited sporadically in the literature, with more

D. Szekely · T. W. Yau · P. W. Kuchel (✉)
School of Molecular and Microbial Biosciences,
University of Sydney, Building G08,
Sydney, NSW 2006, Australia
e-mail: p.kuchel@mmb.usyd.edu.au

P. W. Kuchel
Centre for Mathematical Biology,
University of Sydney, Sydney, NSW 2006, Australia

recent studies using modern digital imaging and processing techniques to characterize underlying frequencies of membrane undulations, reporting a range of 0.2–30 Hz (Krol et al. 1990). The maximum amplitude of the undulations has been estimated at 0.4 μm (Krol et al. 1990), ~5% of the average RBC diameter of 7.5 μm, or 40% of the thickness of the cell of ~1 μm. Attempts have also been made to elucidate the cause of the undulations, but a consensus has not been reached, probably because of the physical nature and numerical structure of the recordings.

Initially, the observed undulations were described as "thermally driven Brownian motion" of the lipid bilayer brought about by molecules colliding with it (Pulvertaft 1949). A correlation between flickering in populations of cells and metabolism/transport was discovered (as early as almost 60 years ago) through the introduction of chemical inhibitors including the –SH-group reagent, iodoacetamide (Blowers et al. 1951). This result implied that flickering in RBC membranes may have an important biological function (Kuchel and Benga 2005).

More recently the mechanism of membrane fluctuations has been ascribed to ATP-dependent phosphorylation of structural proteins associated with the membrane (Levin and Korenstein 1991). This may be the consequence of strongly buffered energy-driven maintenance of cell integrity, postulated to be through the dissociation of actin from spectrin at nodes in the RBC cytoskeleton (Gov and Safran 2005), which could contribute to the energy expenditure that is unaccounted for in human RBCs [~50% of the total ATP flux (Kuchel and Benga 2005)].

Recent work has shown that there is a significant lag period between the depletion of ATP (caused by blocking glycolysis) and gross changes in cell shape through echinocytosis (Pages et al. 2008). The conclusion from the latter study is that fluctuations in the gross RBC morphology are, to a large extent, independent of ATP concentration.

Despite its long history of study, the mechanisms of membrane flickering are poorly understood, despite ascribing a vital cell physiological role to autonomous motion of the RBC and cells in general. We posit that the ability to flicker gives the RBC a self-mediated mechanism which allows it to more easily "wiggle through" the narrow capillaries in the body that measure as little as 4 μm in diameter (Agar and Board 1983), approximately half that of the RBC. The spleen imposes the smallest apertures through which RBCs must pass in vivo: as little as 0.5 μm (Agar and Board 1983). Without their autonomous movements, the flow of RBCs through the bloodstream could much more easily become impeded in these narrow apertures. This hypothesis has been explored previously (Krol et al. 1990) but more evidence is required to assign energy expenditure, and to rule out simple Brownian motion of the lipid bilayer as the basis of flickering (Strey et al. 1995). Another plausible hypothesis is that flickering evolved to reduce the effect of unstirred regions on solute flow within the cell by continuously mixing the cell contents. This is also only conjecture and the physiological relevance of flickering begs further investigation.

The purpose of the present study was to characterize further the dynamics of the membrane flickering phenomenon in human RBCs using DIC microscopy with recently available higher-speed imaging (>300 Hz) than used before, a factor of 10 greater than in Costa et al. (2008). Both new and classical data processing techniques were used to address the following hypotheses: (1) membrane fluctuations are dependent on factors including temperature, ATP concentration, water transport rates, and RBC age; and (2) it is tightly controlled, befitting an important biological function. In perturbing normal conditions in vitro, we aimed to measure changes in the dynamical nature of the fluctuations with a view to understanding the underlying causal mechanisms.

A Monte Carlo computer simulation of the system was constructed which generated a time course of spatial fluctuations with the aim of understanding how numerical perturbations to the system affect the statistical properties of the complex multiscale temporal structure of a typical time series (Blowers et al. 1951). These were then compared with data from RBCs to posit fundamental principles relating to membrane/cytoskeletal properties which give rise to the observed fluctuations.

Materials and methods

D-Glucose, sodium chloride, and sodium dihydrogen orthophosphate were obtained from Asia Pacific Specialty Chemicals Ltd., Sydney, NSW. Heparin was from David Bull Laboratories, Mulgrave, Victoria. α-Toxin (from *Staphylococcus aureus*), bovine serum albumin, glycerol, microscopic latex spheres, manganese chloride, penicillin-G, *p*-chloromercuribenzenesulfonate (pCMBS), poly-L-lysine, sodium fluoride, streptomycin sulfate, and triethyl phosphate were from Sigma Chemical Co., St Louis, MO, USA.

Microscopy experiments

Human RBCs were obtained by venipuncture from the cubital fossa of a healthy donor (D.S.). The cells were washed centrifugally three times (10 min, 3,000×*g*, 5°C) in a solution of isotonic saline consisting of 154 mM NaCl, 10 mM glucose, 283 mOsm kg^{-1}. The buffy coat was removed by vacuum-pump aspiration. The final wash was performed after the addition of 0.5% w/v of bovine serum

albumin (BSA) (pH 7.4) to the isotonic saline solution, and only the topmost fraction was collected for experiments since this fraction contained the youngest RBCs. For the experiments in which young and old RBCs were used, the cells were further centrifuged (30 min, 10,000×*g*, 30°C) and the topmost and bottommost fractions were recovered (Ballas et al. 1986). In all cases the packing density (hematocrit) of RBCs was adjusted to ~0.05. Circular glass coverslips (42 × 0.17 mm) were treated with 2 mM poly-L-lysine (Sigma), the excess of which was subsequently washed off with distilled water. The coverslips were then dried for 3 h at 65°C and treated with 0.5% w/v BSA saline. Aliquots of 40 μL RBCs suspended in 0.5% w/v BSA saline (hematocrit ~0.005) were transferred into an 8-mm-diameter well in a 0.3-mm-thick copper shim spacer, coated with high-vacuum grease, and sandwiched between two coverslips. The sample in the overflow volume served to seal the chamber. The coverslips were fixed into a PeCon perfusion chamber, with solutes perifused using a Gilson peristaltic pump (Gilson Inc., Middleton, WI) and temperature controlled using a PeCon Tempcontrol 37-2 digital unit. The DIC microscopy images were recorded digitally at 20°C, 25°C, 31°C, and 37°C with a 100× oil-immersion objective on a Zeiss Axiovert 200 M microscope, with a monochrome HSm digital camera (Zeiss, Jena, Germany). The images and movies were exported using Stallion software (3i; Intelligent Imaging Innovations Inc., Denver, CO) and these data were further processed using purpose-written algorithms programmed in *Mathematica* (Wolfram Research, Champaign, IL) (Wolfram 2007).

^{31}P nuclear magnetic resonance (NMR) experiments

These were conducted on a Bruker (Karlsruhe, Germany) AMX 400 spectrometer with a 9.34-T wide-bore vertical magnet (Oxford Instruments, Oxford, UK). A 10-mm broadband probe was used with the inner coil tuned to the resonance frequency of ^{31}P, and the outer coil to the frequency of ^{1}H. Triethyl phosphate (TEP) of a known concentration was added to all samples as a ^{31}P chemical-shift (0.44 ppm) and intensity reference (4 mM) (Kirk et al. 1986). Spectra were acquired with rapid radiofrequency (RF) pulsing and continuous broadband proton decoupling (WALTZ-16) (Shaka et al. 1983). The acquisition time was 0.34 s and the spectral width was fixed at 6,000 Hz; and the relaxation delay was 1 s. The number of transients per spectrum was 630 with an experiment time of 15 min; the signal-to-noise ratio of the ATP-γP peak at the beginning of the experiments was 10 and 14, at 25°C and 37°C, respectively. The variable temperature unit was set to 23°C or 35°C to give sample temperatures of 25°C or 37°C, respectively, due to the heating associated with broadband decoupling. Free induction decays were zero-filled with 8,192 data points, and 6 Hz exponential multiplication was applied before Fourier-transforming the data.

Water transport

The water exchange time (T_e) was measured by a Mn^{2+}-doping ^{1}H nuclear magnetic resonance (NMR) method (Conlon and Outhred 1972) on a Bruker Mini-Spec MQ20 operating at a frequency of 20 MHz for ^{1}H nuclei, as previously described (Benga et al. 2002). Briefly, samples for NMR measurements of the water proton relaxation times (T_{2e}'; the prime denotes the fact that this is a composite relaxation time) were prepared by gentle mixing of 0.4 mL RBCs and 0.2 mL doping solution (40 mM $MnCl_2$, 100 mM NaCl). The transverse relaxation time of the water in the cell interior (T_{2i}) was measured on packed cells (hematocrit >95%) from which the supernatant, with no added Mn^{2+}, had been removed by centrifugation. As shown by Conlon and Outhred (Conlon and Outhred 1972), T_{2e}' and T_{2i} are the parameters that are required to estimate the water diffusion exchange time, T_e, by using the equation:

$$\frac{1}{T_e} = \frac{1}{T_{2e}'} - \frac{1}{T_{2i}}. \quad (1)$$

Brownian motion

Solid latex spheres (~15 μm in diameter) (Sigma) were prepared and images recorded using the same method as for RBCs, except the spheres were not attached to the coverslips. They were suspended in BSA saline and adjusted to temperatures of 20°C, 25°C, 31°C, and 37°C and images were recorded using a 100× oil-immersion objective on the Zeiss Axiovert 200 M microscope with a monochrome HSm digital camera, as above.

Theory of methods

In the following section, various data processing techniques, some of which have been used previously to characterize RBC flickering (Costa et al. 2008), are outlined in order to give our implementations and extensions of them in *Mathematica*. These were applied to the data, the results of which are summarized in Figs. 1 and 2.

Synthetic noise

To generate synthetic data for use in testing the data processing algorithms, white and red noise were generated using the following function (Coza and Morariu 2003; Gardiner 2004);

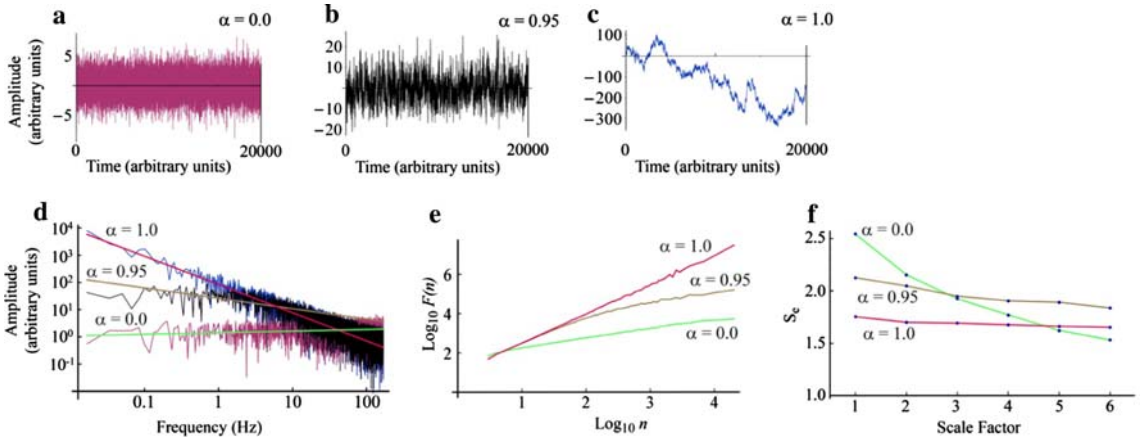

Fig. 1 Synthetic white- and red-noise data generated using Eq. 2 **a–c** show time series generated using $\alpha = 0.0$ (*pink*), 0.95 (*black*), and 1.0 (*blue*), respectively; and **d–f** show power spectra, DFA, and MSE analyses of these data, respectively. The *red*, *tan*, and *green* trendlines correspond to $\alpha = 0.0$, 0.95, and 1.0, respectively

$$f(t) = \sum_{i=1}^{N} \alpha f(t_{i-1}) + \mathcal{N}(\mu, \sigma), \tag{2}$$

where N is the length of the time series, α is the correlation coefficient, and $\mathcal{N}$ is a random, normally distributed, real number with mean μ and standard deviation σ. The time series was described as white noise when $\alpha < 1$ and red noise when $\alpha = 1.0$. Examples of the noise produced by this method are shown in Fig. 1a–c, with $\alpha = 0.0$, 0.95, and 1.0. The values of $\mathcal{N}$ were generated in *Mathematica* using Rule 30 of the one-dimensional cellular automaton (Wolfram 1983).

Power spectrum

The Fourier transform (see Appendix), $X(f)$, was computed according to Eq. 5, on a Log–Log scale, and nonlinear regression used to fit a straight line to the spectra. For brevity, these are hereafter referred to as "power spectra." To account for white noise, data were weighted such that the weight at frequency f, was $e^{-0.15f}$.

Applying power spectrum analysis to synthetic red noise data, generated using Eq. 2, yielded trends that were nonlinear and linear (with a slope of 1.0), respectively (Fig. 1d). The information obtained from the slope pertains to the rate of decay of the amplitude of the Fourier transform versus the corresponding frequency.

Mathematical model

A computer simulation was developed to facilitate understanding of the numerical structure of the time series that were obtained from real flickering cells. The model was based on an idea that is best described by analogy: membrane measurements of flickering can be visualized as if the monitored pixel is a buoy in an ocean. The buoy is impacted upon by waves propagating from sources randomly placed around it, and it responds by a change in its altitude from sea level. The time course generated by sampling the buoy's altitude (at time intervals δt) is:

$$\sum_{i=1}^{N} f_i(r, s), \tag{3}$$

where N is the length of the time series, and is equal to the total sampling period divided by δt; f_i is the ith wave that the buoy encounters; l is the duration of wave f_i (l was chosen to be the time at which f_i decays to 1% of its initial value); r is the time at which the buoy encounters the ith wave; and s is the magnitude of the wave. In other words, the time series is the superposition of all the waves that the buoy encounters over the sampling period. The choice of $N + l$ iterations of f_i was arbitrary but it allowed for an average of one wave per time point. The time courses and power spectra did not change significantly beyond $\sim N/4$ iterations of f_i. For the simulations, t was a randomly chosen integer such that $1 - l \leq r \leq N$, and s was a randomly chosen real number such that $-1 \leq s \leq 1$. The following empirical function described the wave f_i:

$$f_i = (t - r)^{-\aleph} \mathrm{e}^{-0.00195(t-r)\times s}, \tag{4}$$

where t is time; and $\aleph$ (i.e., alef) is interpreted as a physical rigidity factor.

Results

See the Appendix for a discussion, in the present context, of the Fourier transform, wavelet transform, magnitude mode, DFA, and multiscale entropy analyses.

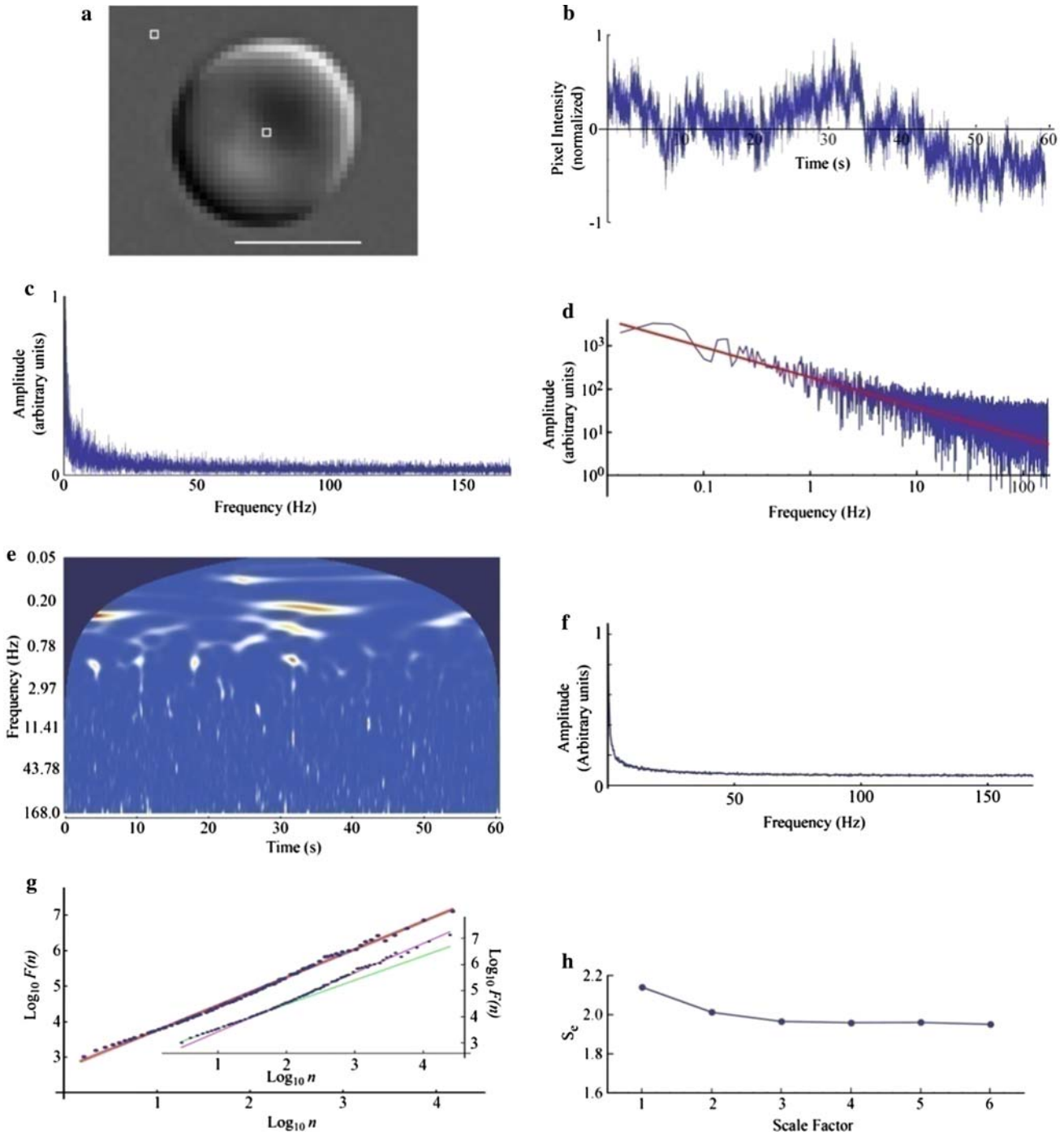

Fig. 2 RBC flickering analysis methods. **a** A typical discocytic RBC chosen for analysis. The *empty white squares* indicate the regions of interest (ROIs); the one outside of the cell was used for detrending the data acquired from the ROI in the center of the cell. The *scale bar* indicates 5 μm. **b** Typical time series acquired from the RBC central ROI after detrending; and **c** and **d** are its Fourier transforms on a linear scale, and Log_{10}–Log_{10} scale, respectively. The *thick red line* through **d** is the least-squares best fit using exponentially decreasing weights, and has a slope of −0.618. **e** Wavelet transform of **b**; *blue* indicates zero to low power, *white* indicates mid-level power, and *red* indicates high power; and the *dark blue* cone around the outside of the data is the "cone of influence" (Torrence and Compo 1998). **f** Magnitude-mode spectrum of data similar to **b** (see text). **g** Detrended fluctuation analysis (DFA) of the data, with slope of 1.10 indicated by the thick red line; inset shows the same data with two lines fitted with slopes of 0.94 and 1.14 indicated by the *green* and *purple lines*, respectively. **h** MSE analysis of the data in **b** with complexity index (Costa et al. 2008), 12.11

Pixel intensities

Time-lapse DIC microscopy recordings (20,000 frames at ~336 frames s^{-1}) of fresh RBCs were analyzed. Figure 2 gives a summary of the data processing techniques that were used. Figure 2a shows a frame from a typical RBC time course at 37°C using the 100× oil-immersion objective. It represents a matrix of 12-bit numerical pixel intensity values that were determined by the difference in thickness of the imaged object (measured along the vertical axis) between the beams of light split by the Nomarski prism in the DIC microscope (Cogswell and Sheppard 1992). Four-pixel binning enabled an increase in the rate of image capture by decreasing the camera exposure time to 1 ms. The region of interest (ROI) within the RBC, indicated by the white square, was monitored over time, and the square next to the RBC was the pixel used for baseline correction. The data series (Fig. 2b) had pixel intensities that oscillated randomly about a mean value, with a long-period baseline.

Fourier transform

Figure 2c shows the Fourier transform of the time series of Fig. 2b, with its exponentially decreasing amplitude as frequency decreases; this is a so-called red noise spectrum (Gardiner 2004; Milotti 1995). Note the absence of any distinct resolved peaks in the Fourier transform of the data. Thus, there is no single frequency at which the RBCs flickered over the entire time course; instead there was a range of frequencies, most prominently between 0.015 and 10.0 Hz. However, there appeared to be weak signals between ~10 and 60 Hz, and white noise beyond ~60 Hz.

Power spectrum

Figure 2d shows the power spectrum analysis of the flickering time course. This type of analysis had been used previously to interpret red noise fluctuation data from cells (Coza and Morariu 2003). Here, the analysis was extended by fitting a line to the RBC data, to metrify the red noise; and exponentially decreasing weights were used to account for the white noise in the Fourier spectrum. This noise was visibly prevalent and interfered with the fitting of the power spectrum at frequencies lower than ~5.5 Hz; this was evidenced by the gradually increasing cone of amplitude values beyond this frequency. These data yielded a slope (the characteristic metric) that was used to compare spectra between different experiments.

Wavelet transform

To detect temporally localized signals of a particular frequency, the Morlet wavelet transform was applied to the time series (Fig. 2e; blue color code indicates zero to low power, white indicates mid-level power, and red indicates high power). The analysis showed that there were sparsely spaced peaks representing several frequencies that could be resolved; however, the lack of extended contiguous high-power peaks implied that there was no single frequency at which the RBCs flickered. The wider, high-power peaks toward the top of the two-dimensional (2D) spectrum corresponded to frequencies (~0.2 Hz) that were lower than those expected for flickering. These peaks were attributed to gross movements in the position of the cell, possibly caused by thermally driven water currents.

Magnitude-mode spectrum

The magnitude-mode spectrum shown in Fig. 2f was obtained by acquiring 100 × 10 s (3,360 frames) of ROI data for an individual cell. Image acquisition was started and stopped after 10 s, then the camera view was autofocused using a Laplacian method in the Stallion software, taking ~4 s; the process was repeated 100 times. The analysis exposed a range of low frequencies, but there was no single resolved peak. Again, the conclusion from these data was that there was no characteristic frequency at which the RBCs flickered.

Detrended fluctuation analysis

When applied to the data in Fig. 2b, the DFA (Fig. 2g), produced a series of points that had an upward trend, going from left to right. A single line was fitted through these data, but a higher-degree fit, using two line segments (illustrated in Fig. 2g inset), gave a better description of the data. This was also the case when DFA was used to analyze heart interbeat interval data from normal and congestive heart failure patients (Peng et al. 1995). This behavior was identified and has been explored previously (Morariu et al. 2007); however, an explanation for it remains elusive. The behavior was consistent with all of the data obtained from the flickering experiments; the difference between the slopes of the two curves was on average ~13%. Moreover the position of intersection between the two lines varied between time courses. Because of this, a robust metric that allowed comparison between experiments using this method was not achieved.

Multiscale entropy analysis

MSE analysis produced a curve with exponentially decreasing entropy as the scale increased, with a positive offset baseline (Fig. 2h) that differed between cells. Costa et al. (2008) integrated the curve over each of the six scale values to produce a metric-value called the "complexity

index," and this was used to compare their experimental results. This metric disregards the profile of the MSE curve that contains information about the decay of entropy as the scale value increases.

Power spectrum analysis was used to compare time series from different experiments. A justification for this is provided in the "Discussion".

Temperature/Brownian motion

Individual RBCs and latex spheres were monitored at different temperatures to determine whether the analysis of the flickering time series was affected (results summarized in Fig. 3a). Vibrations from refrigeration devices would have interfered with the results, so all cooling was performed with a heat block attached to an ice-cooled-water gravity delivery system. Each cell and latex sphere was first recorded at 20°C, then 25°C, 31°C, and 37°C and finally back to 25°C. For RBCs, at 20°C, the slopes of the power spectra plots were on average ~6% less than at 25°C. There was little change in slope between 25°C and 37°C. Thus the temperature changes imposed on the RBCs had an insignificant effect on the metric from the power spectra (Fig. 3a, solid line). The latex spheres on the other hand responded to the changes in temperature more noticeably with a systematic decrease in the absolute value of the power spectrum slope with increased temperature (Fig. 3a, dashed line). It is worth noting though that the recorded time courses and Fourier spectra appeared similar to those of the RBCs.

ATP concentration

Assessment of the dependence of flickering on ATP concentration was performed in two ways: (1) through the addition of 154 mM sodium fluoride to fresh cells at 37°C, which blocked enolase, and hence inhibited glycolysis (Kuchel et al. 2004) and caused ATP depletion in ~1.5 h (Pages et al. 2008), and (2) through the addition of α-toxin from *S. aureus* to fresh RBCs, which brought about ATP permeability of the RBCs, allowing serial dilutions of the ATP concentration in the suspension. Both experiments were performed in parallel with equivalent ^{31}P NMR experiments to confirm complete depletion of intracellular ATP. The former experiment was performed so that an individual cell was monitored at 37°C before, and every 30 min for 2 h after, addition of sodium fluoride, and then again after isotonic saline was perifused. The monitored cells were visibly undergoing echinocytosis with type 2 or 3 echinocytes [a classification scheme based on Bessis (1972) was used] forming within the 2 h incubation. Cells which evolved further than this, i.e., type 4 or 5 echinocytes,

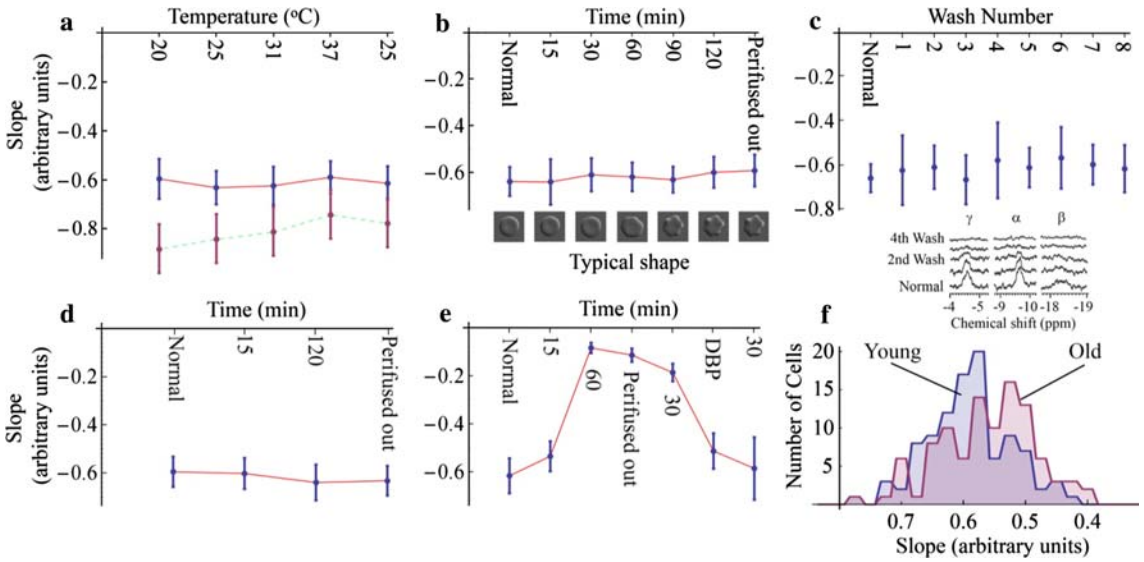

Fig. 3 Power-spectral analysis of data acquired from RBCs under various experimental conditions. **a**, **b**, **d**, **e** Show the results obtained from each individual cell (**a**) (*solid red line*) and each latex particle (*dashed green line*) monitored at 20°C, 25°C, 31°C, and 37°C and then again at 25°C; **b** with NaF added, and then perifused out after 2 h (inset shows the morphology of one of the cells used in the analysis; flickering was present in cells undergoing echinocytosis); **d** with the addition of 20% glycerol; and **e** with the addition of pCMBS and subsequent addition of dibutyl phthalate (DBP). The *red line* is to guide the eye and indicates that the same cell was monitored after the perturbation of normal conditions. **c** Results obtained from cells which have undergone treatment with α-toxin from *S. aureus*. The inset shows the γ-, α-, and β-peaks of ATP from the corresponding ^{31}P NMR spectra. Each successive wash reduced the intracellular ATP concentration by ~50%. The same individual cells could not be monitored due to hemolysis occurring in the suspension. The error bars indicate the standard deviation of the estimate of the metric. **f** Histogram showing the slopes of the young (*blue*) and old (*red*) populations

detached from the glass coverslip, and so were not considered. Despite morphologically evolving, the cells gave approximately the same power spectrum metric as they did prior to incubation with NaF (Fig. 3b). Their morphology was unchanged after the NaF was replaced with saline.

Individual RBCs could not be monitored in the α-toxin perifusion experiments since lysis was prevalent at low hematocrits. Instead, a suspension of packed cells (ht ~0.9) was incubated with α-toxin, then centrifugally washed in two volumes of ATP-free phosphate buffered saline (PBS), and fractions removed for microscopy (repeated eight times). The cells did not undergo echinocytosis despite being depleted of ATP (confirmed using ^{31}P NMR). Again, the power spectra metrics did not change by a significant amount between the time courses for the α-toxin experiments (Fig. 3c).

RBCs that had been metabolically perturbed in vitro to the extent that they were spherocytosed (e.g., after the addition of hexafluoride) did not flicker. A blood donor, however, with hereditary spherocytosis produced cells that not only responded normally with volume changes in response to changes in osmolality, and morphology changes in response to interaction with borosilicate glass, but also flickered normally (detailed results not shown).

Water transport

Perturbations in water transport were also made in two ways, namely, perifusion of: (1) 20% glycerol and (2) pCMBS [10 nmol (mg membrane)$^{-1}$] (Benga et al. 1986) into a suspension of fresh RBCs. Both were performed so that individual cells were monitored before and after the addition of the interfering substance. Glycerol exerted an insignificant effect on the RBC flickering time courses and analyses (Fig. 3d); however, pCMBS caused cessation of flickering after incubation for 30 min at 37°C. Dibutyl phthalate (DBP) was subsequently perfused into the suspension, causing the monitored cells to flicker again (Fig. 3e).

There was an increase of ~45% in the mean residence time of water in pCMBS-treated cells after 30 min at 37°C estimated using NMR spectroscopy, and a subsequent decrease in mean residence time of ~300% after incubating cells with 5 mM DBP for 40 min at 37°C.

Cell age

Upon high-speed centrifugation, a suspension of RBCs in saline became partitioned with the densest (oldest) cells sedimenting to the bottom of the cell pellet, while the least dense (youngest) moved to the top (Ballas et al. 1986). To determine the effect of cell age on the characteristics of flickering, time courses of 100 young and 100 old cells were recorded at 37°C (Fig. 3f). Cell age had a small effect on the average power spectrum metric in both populations (the average metric of the old cells was ~9% lower than the young cells). The range of values in the old population was significantly higher (~55%). To test the statistical null hypothesis that the two populations were indistinguishable from one another, a Wilcoxon rank-sum test with continuity correction and a Welch two-sample t test were used. The analysis returned P values of 0.0012 and 0.0031, respectively, and led to rejection of the null hypothesis.

The following hypothesis/question was also tested: given an individual cell from either population, could it be determined from the analyses if the cell is young or old? For this, the cumulative distribution functions of the two populations were used. This yielded a P value of 0.551; hence there is only a ~50% probability of being certain that a cell is from either the young or old population.

Mathematical simulation

The details of the flickering model are given in the "Theory of methods." It was based on the idea that waves propagate from sources on or just below the cell surface, like an earthquake under the ocean.

The consequences of RBC aging were simulated, using Eq. 4, by varying the value of the rigidity factor, ℵ, from 0.35 to 0.43 for new and old cells, respectively, with $N = 20{,}000$. For comparison, simulations using $\aleph = 0.1$, 0.7, and 1.0 were included and are summarized in Fig. 4. Simulated data were processed in the same way as for the real RBC measurements. Performing the simulation 100 times was expected to yield approximately the same power spectrum metric for each simulation, however an average slope of -0.623 ± 0.049 and -0.551 ± 0.051 was measured for the new and old cells, respectively (these values were comparable with those obtained from the DIC microscopy experiments). The histograms in Figs. 4e and f show that the simulation yielded a metric of -0.713, and then at a different time with the same parameters yielded a metric of -0.468, a phenomenon also observed in the RBC experiments. This result brings to light the complexity and randomness of the recordings of flickering that were acquired.

Figure 4a shows a comparison of the waves used to generate the time courses. It shows that the rate of decay of the wave is proportional to the rigidity factor, and is analogous to waves through the RBC membrane.

Figure 4b–d shows the effect of the contributions from white noise highlighted by the black data (generated by the camera in the RBC experiments; the level of this noise was determined empirically).

Figure 4d shows the efficacy of the fitting method, which yielded a metric that was unaffected by the synthetic noise. Line fitting of synthetic-noise-free data is indicated

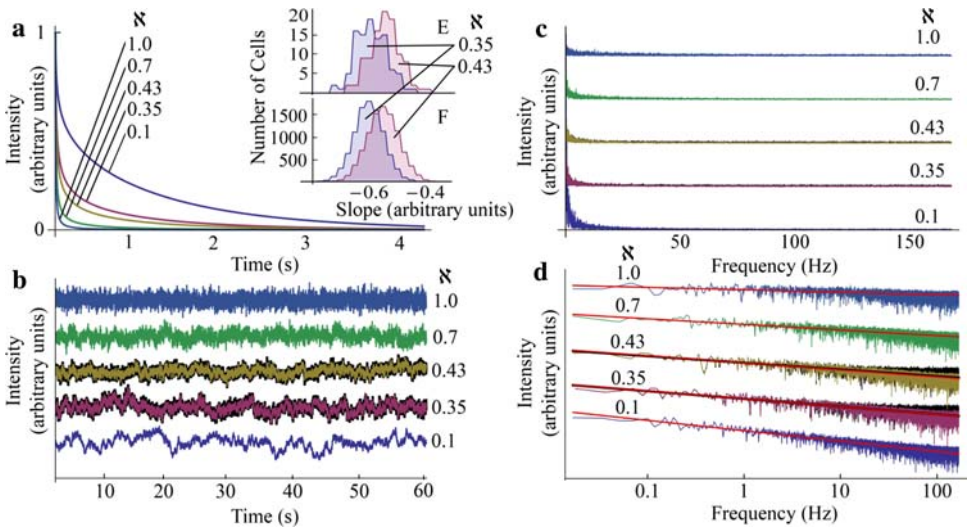

Fig. 4 Computer simulations of RBC flickering using Eq. 4 with rigidity factors, $\aleph = 1.0$ (*light blue*), 0.7 (*green*), 0.43 (*tan*, represents old cells), 0.35 (*pink*, represents young cells), and 0.1 (*dark blue*), respectively. **a** Shape of the slope-perturbing wave that was used for each of the time courses in (**b**). **c** and **d** Corresponding Fourier transform and power spectra with slope for the fitted lines (*thick red line*, and *thick black line* for those with noise) of −0.195, −0.446, −0.565 (−0.534 with noise), −0.621 (−0.615 with noise), and −0.827, where $\aleph = 1$, 0.7, 0.43, 0.35, and 0.1, respectively. The black data in **b** and **d** for $\aleph = 0.43$ and 0.35 represent synthetic noise added to the time course to simulate noise originating from the camera in the DIC microscopy experiments. The histograms in **e** and **f** show the results of running the simulation 100 and 10,000 times, respectively, for both $\aleph = 0.43$ (*red*) and 0.35 (*blue*)

by the thick red line, while the noisy data are indicated by the thick black line.

Figure 4e, f shows simulations of the age population study $\aleph = 0.43$ (old cells) and 0.35 (young cells) for 100 and 10,000 cells, respectively.

Discussion

Membrane flickering is a readily visualized process, and yet it is poorly characterized and its underlying mechanisms are poorly understood. It occurs in many cell types: nucleated and nonnucleated including monocytes, lymphocytes, 3T6 fibroblasts, cardiomyocytes (Krol et al. 1990), murine lymphoma B and T cells (Mittelman et al. 1991, 1994), and protoplasts (Miller 1963). It has previously been shown to be affected by cell age (Costa et al. 2008) and cellular ATP concentration (Gov and Safran 2005). Indeed, it was determined that the only prerequisites for a cell to display flickering are: (1) zero surface tension, (2) high fluidity of the cell interior, and (3) inequality of refractive indices of the extra- and intracellular compartments (Brochard and Lennon 1975). Our experiments were performed using advanced image processing techniques that enabled exploration of the possibility of temperature and water transport affecting flickering properties. A computer model was developed to examine the numerical structure of the acquired time series. Because of the high variability of the slope of the power spectra, measured in the cell age experiments, perturbations in the flickering of individual cells, rather than populations of cells, were measured in most of the experiments.

One of the seminal papers on RBC flickering (Brochard and Lennon 1975) showed successfully for the first time that the observed fluctuations could be quantified by measuring (1) the mean amplitude of the cell thickness fluctuations, (2) the frequency spectrum, and (3) a two-point spatial correlation function. We focused on the frequency spectrum measurement of RBC flickering since this was the most straightforward to acquire and to compare between samples, and also since this paper contains a fundamental flaw in their analysis of the data. They fitted a straight line to the high-frequency part of the frequency spectrum, which we showed contains noise of sufficient amplitude to interfere with straight-line fitting.

The following section gives justification for the image acquisition and data processing techniques used in our study.

Image acquisition

Previous studies: (1) used phase contrast and (2) chose pixels at the boundaries of the cell (Costa et al. 2008; Gov and Safran 2005; Strey et al. 1995). In the present work, for each imaged cell, only the pixel that was closest to the center of the cell's dimple was chosen, since this is the largest region of the cell where the normal to the surface is facing directly toward the camera. It represented an area of

$\sim$77 nm^2. This area was chosen so that cell movements and gross volume fluctuations did not interfere with the recorded time courses of fixed light intensity. Only contributions from small, localized volume fluctuations and membrane undulations were therefore recorded. It is clear that the effect of gross, whole-cell movement by Brownian motion will be superimposed on true membrane flickering if a pixel at the edge of the cell is the source of the time series, as opposed to the flat depression in the center of the cell that was used. This area also produced the greatest average values in the range of pixel intensities, over the time courses. Increasing the voxel size (from a 1 $\times$ 1 pixel to 2 $\times$ 2 or 3 $\times$ 3 pixels) had little effect on the form of the acquired data over a time course. The choice of a 1 $\times$ 1 pixel minimized the effect of movements of the cell, which were observed even with poly-L-lysine treatment of the glass coverslips.

The preference for the use of DIC microscopy over other optical methods is based on three of its features: (1) DIC microscopy produced greater contrast from RBC samples, which is reflected in the range of relative pixel intensities produced by the two methods (in 300 frames of acquired data, phase contrast produced a dynamic range of 82, while DIC microscopy produced a dynamic range of 185 pixel intensity values), (2) the acquisition time for DIC microscopy images was significantly less (for comparison, the light intensity was fixed, and the acquisition time adjusted to maximize the dynamic range of the camera for an RBC under phase contrast and DIC; acquisition times were 367 and 69 ms, respectively), allowing both greater acquisition rates and minimizing photochemical damage to the cells, and (3) unlike phase contrast, DIC microscopy does not produce size/halo artifacts in the RBC samples, so the images do not require postprocessing.

Note that both phase contrast and DIC microscopy rely on the thickness and refractive index of a sample in order to generate contrast in the image. DIC could not be used, however, to measure the actual amplitudes (distances moved) of fluctuations since factors such as baseline pixel intensity varied from one cell to the next. The time courses were baseline-corrected by subtracting the trend given by the pixel intensities from a region of interest (ROI) outside of the cell (the empty white square next to the RBC in Fig. 2a) to account for changes in average light intensity, prior to data processing.

Data processing

The only technique that emerged as potentially containing discriminatory information, useful for comparing flickering of RBCs of different ages, and under different experimental conditions, was power spectrum analysis. The power spectrum analysis produced a metric (the slope) for each experiment allowing ready comparison between cells under various experimental conditions. To ascertain whether the information obtained from this analysis was different from DFA or MSE analysis, young and old RBCs were studied.

Evaluation of numerical properties of DFA, MSE, and power spectrum analysis

One hundred cells from both the young and old populations were studied using the three techniques mentioned in the heading. The analysis produced a large range of values for both populations, and the metrics overlapped (Fig. 3f). For this comparison, pairs of time series were considered (one from the young and one from the old population) which produced power spectrum metrics that were within 1% of each other. In other words, only the time courses from which the analyses of a young cell and an old cell resulted in approximately the same metric were considered.

DFA and MSE analysis were compared to determine whether they provided different information about these cells than the power spectrum. Assuming that this was the case, the difference between the cells from the two different populations would be >1%; however, this was not the case. The slope of the line fitted to the DFA graph changed by an average of 47% less, and the MSE complexity index changed by an average of 62% less, than the power spectrum metric. This implied that the DFA and MSE analysis yielded no more information about the time series than the power spectrum. For completeness, all three techniques were applied to all of the data acquired in the study. Consistently, between time series, an increase in power spectrum metric correlated with an increase in DFA and a decrease in MSE metrics.

None of the three techniques took into account amplitude of fluctuations, only relative Fourier power decay as frequency increased in the case of power spectrum analysis, relative residuals between different scales of detrended data in the case of DFA, and long-range correlations in data in the case of MSE. The main quantifiable difference between the three techniques was computation time, which was significantly less for the power spectrum analysis. Therefore this technique was used to analyze subsequent time series.

Time series variability

There was a high degree of variability between different time courses, reflected in the analysis of the time series acquired for the magnitude-mode processing. Imaging data from a single cell (100 $\times$ 10 s, each separated by $\sim$4 s for autofocusing) gave an average power spectrum metric of -0.599 ± 0.053. Greater variability was

encountered in the experiments in which data were recorded from different cells, e.g., the different average metrics of -0.612 ± 0.69 and -0.556 ± 0.075 for young and old cells, respectively.

Although the trends in the power spectra obtained from RBCs were linear, the slopes were <1, implying that the recorded time courses were not simply describable as red noise. A simple interpretation is that the metric would be affected by the rigidity of the RBC membrane since the amplitude of fluctuations through a stiffer membrane would more rapidly decay because of elastic dampening. This idea was explored further and is described in the final section under "Mathematical simulation."

Temperature

Increases in temperature have a marked stimulatory effect on the activation and steady-state kinetics of all enzymic and chemical processes in RBCs (Agar and Board 1983; Bernhardt and Ellory 2003; Khan et al. 2000), as well as the kinetic energy of particles undergoing Brownian motion (Einstein 1905) and the flexibility of the lipid bilayer (Garrett and Grisham 1999). Passive cation permeability in RBCs, however, has been shown to increase at low temperature (Stewart et al. 1980). The present results of flickering analysis of RBCs indicated that temperature had an insignificant effect on the spectral features of flickering.

RBCs: There was a small change in the slope of the power spectra from each individual cell between 20°C and 25°C, and an insignificant change in the slopes of the power spectra of these cells from 25°C to 37°C, (Fig. 3a, solid line). The interpretation of this was: (1) while the rate of frequency decay may have been approximately the same between experiments, other factors may have been influential, such as fluctuation amplitude, which cannot be measured directly using the DIC methodology, and (2) motility is important for RBC survival; so changes in environmental temperature may be accounted for by an, as yet, unknown process. This unexpected result has been shown previously (Fricke and Sackmann 1984). However it was worthwhile confirming such an important result with more recent imaging technology and modern data processing techniques.

Latex spheres: Upon changing the temperature of the system, the Brownian motion of the latex spheres (which was clearly visible when viewed under the microscope) changed significantly, as shown by the dashed line in Fig. 3a. We interpreted the decrease in the absolute value of the slope as implying that the higher frequencies were more prominently represented at higher temperatures. Therefore, the rate of exponential decrease in Fourier amplitude versus frequency had decreased.

ATP concentration and cell pathology

The dependence of cell membrane fluctuations on ATP concentration has been the subject of previous studies (Gov and Safran 2005; Levin and Korenstein 1991; Tuvia et al. 1998). It is claimed that ATP-depleted cells flicker with lower amplitudes than fresh cells or ATP-repleted cells. Moreover, the inhibition of cellular ATPases was reported to reduce flickering amplitude, though this result has recently been disputed (Evans et al. 2008).

Spectrin association/dissociation: Gov and Safran (2005) proposed that the transient, rapid, ATP-dependent dissociation/association of spectrin filaments from actin in the RBC cytoskeleton could account for the observed membrane flickering. They posited that the cell expends significant amounts of energy through the hydrolysis of ATP in order to increase the amplitude of the membrane fluctuations, and these aid in overall cellular motility.

A protrusion of $\sim$40 nm occurs when one spectrin molecule transiently dissociates from the hexagonal-junction network (Gov and Safran 2005). Flickering-based protrusions of $\sim$400 nm occur in RBCs (Krol et al. 1990), so a minimum of 271 of these junctions are required (assuming that all of them collapse either inwards or outwards), or $\sim$2,500 spectrin molecules to produce displacements of distances in the range measured by DIC microscopy. However, synchronization of the dissociation/association of spectrin molecules on this scale is unlikely to occur, and so alone cannot account for RBC flickering. However, our results cannot invalidate those conclusions drawn in the above-mentioned articles since we were only able to measure flickering frequency, and not amplitude. In other words, it is conceivable that ATP consumption plays a role in RBC flickering amplitude; however, our recordings and analysis were unable to detect it.

Hereditary spherocytosis: This condition is characterized by defects in the genes that code for proteins involved in cytoskeleton composition and maintenance, including spectrin, actin, band 3, protein 4.1, and most commonly (and in the case of the above-mentioned blood donor with hereditary spherocytosis) ankyrin (Gallagher and Forget 1998), which mediates the attachment of integral membrane proteins to the spectrin-actin-based cytoskeleton (Bennett and Baines 2001). These RBCs are typically smaller in diameter ($\sim$5 μm) and are less flexible because of membrane loss (Agar and Board 1983). Assuming that flickering is facilitated by ATP-dependent dissociation of spectrin, abnormalities in these integral cytoskeleton proteins would likely perturb flickering. Indeed Krol et al. (1990) found that these cells flicker with a lower amplitude, but this is more likely to be due to the increase in lipid membrane tension than dysfunctional spectrin ATPases. This implies that the cytoskeleton and specifically

spectrin-associated ATPases are not involved in facilitating flickering.

NaF and α-hemolysin: NaF blocks enolase and inhibits glycolysis (Kuchel and Benga 2005), causing ATP depletion and echinocytosis over ~2 h (Blowers et al. 1951). These cells flickered normally over the period that they were monitored (Fig. 3b), indicating that transition to echinocytes type 2 and 3 have an insignificant effect on flickering.

α-Toxin normally exists as a monomer, and integrates into lipid membranes (Bhakdi and Tranumjensen 1991), where it forms a heptameric pore [creating a pore of diameter ~5 nm and height ~9 nm (Gouaux 1998), which allows hemoglobin leakage] through which normally impermeable molecules such as ATP can diffuse (Lind et al. 1987). Repeatedly centrifugally washing the cells in two volumes of ATP-free physiological saline caused a significant reduction in the intracellular ATP concentration (confirmed with ^{31}P NMR), and after ~4 repetitions, the signals from the α-, β-, and γ-peaks in the NMR spectra were too low in signal-to-noise ratio to detect (Fig. 3c), indicating an ATP concentration $<\sim$0.3 mM. For the microscopy experiments, the suspension was washed eight times to ensure depletion of intracellular ATP, and the flickering was monitored after each wash. These cells did not form echinocytes, possibly due to the pores relieving tension on the lipid membrane. Again, the flickering remained relatively constant (Fig. 3c). There was greater variability in these experiments since individual cells could not be monitored. These results imply that flickering is independent of ATP concentration.

Water transport

Every intracellular water molecule in an RBC is replaced ~100 times a second through membrane-inserted aquaporins AQP1 and AQP3 (Roudier et al. 1998; Yang et al. 2001). Unlike AQP1, AQP3 is resistant to pCMBS, which explains the small mercury-insensitive component of water permeability, and is permeable to glycerol (Bernhardt and Ellory 2003). AQP1 is more abundant, with ~120,000–160,000 copies per cell (Yang et al. 2001). Water exchange in human RBCs is known to be much faster than is seemingly necessary (Kuchel and Benga 2005). It has been hypothesized that this high rate may be related to facilitating membrane fluctuations (Kuchel and Benga 2005). Water transport may influence RBC flickering by causing localized volume fluctuations due to inhomogeneities in water flux.

Increasing the viscosity of the medium with 20% (v/v) glycerol had little effect on the features of flickering (Fig. 3d) and brought about only a small change in water mean residence time (~6% higher than normal).

pCMBS gradually inhibited flickering in all RBCs over ~30 min (Fig. 3e). pCMBS is membrane impermeant and reacts selectively with sulfhydryl groups. It can therefore bind to proteins in the RBC membrane including AQP1 and decrease water exchange rate by ~50% (Benga et al. 1986). pCMBS is nonspecific, however, and inhibits nucleoside transport in rat RBCs (Jarvis and Young 1986) so the inhibition of flickering may be due to binding to many other proteins, thus rigidifying the membrane.

The cells maintained their discocyte shape throughout typical time courses and were stable over the 3 h that they were monitored. They did not flicker after washing the excess pCMBS out of the suspension with PBS. They did flicker, however, after perifusing 5 mM DBP [and to a lesser extent, diethyl phthalate (DEP)] into the suspension (flickering was unchanged in fresh cells incubated with DBP or DEP). DBP is used as a plasticizer and can be used, like its analogue DEP, to separate RBCs from water in a saline suspension (Hansen et al. 2001). RBCs in vivo, which had been treated with DEP, had a longer lifespan than those that were not treated (Lovric et al. 1985). Therefore, it was concluded that DEP integrates into the membrane and increased filterability. The mean residence time of water in cells treated with pCMBS was increased by ~45%, but the addition of DEP and DBP caused it to markedly decrease, while staying unchanged in cells that were incubated only with DEP and DBP. These results indicate a strong link between water transport through the RBC membrane, and flickering in RBCs.

Cell age

The differences in flickering between old and young RBCs have been the subject of a recent study (Costa et al. 2008). The motivation for the work is the identification of those features of the RBC that determine its survival in the circulation. RBCs are formed and released from the bone marrow and circulate for ~120 days before they are destroyed. Circulating RBCs therefore represent a full range of young and old cells. Toward senescence, a number of processes occur, including membrane loss and an increase in cell density and stiffness (Waugh et al. 1992). Indeed, there must exist markers associated with the RBC toward the end of its life to facilitate targeting for destruction via the spleen; this appears to be the cell's filterability (Agar and Board 1983). We aimed to elicit differences in flickering characteristics between young and old cells using the analysis.

Costa et al. (2008) found that there were demonstrable differences between the two populations using DFA and MSE. However, with our data, these techniques proved to be non-discriminatory for metrifying cells of different ages.

Similar experiments were performed and processed using power spectrum analysis and, on average, while both populations produced very similar results, there were subtle differences in the two, as shown in the histogram of values in Fig. 3f. The imaging techniques were different from those used by Costa et al., i.e., a greater imaging rate (336 Hz cf. 34 Hz) as well as a larger voxel size (77 nm^2 cf. 4 nm^2); however, this had little apparent impact on the form of the time series.

Our conclusions are that: (1) the populations were different to an extent that they were distinguishable from one another; however, (2) assuming a homogenous field of young and old cells, it is impossible ($\sim$50% probability of getting the correct assignment) to determine from the analysis whether an individual observed cell is young or old. While cell age had a measurable effect on flickering when populations of cells were compared, the differences were insufficient to be able to predict the age of an individual cell. This showed that flickering is buffered to an extent that vast differences in cellular age (at least 100 days, >80% of an RBC's entire lifespan) are insufficient to perturb it significantly.

Varying the temperature of the suspension between 20°C and 37°C had an immeasurable effect on flickering. This was also evident in experiments where cellular ATP was depleted and medium viscosity increased with 20% glycerol. Permanent cessation of flickering was achieved when cells were incubated with pCMBS, and a further recovery of flickering with DBP.

Mathematical simulation

The purpose of the computer model was (for the first time to our knowledge) to provide insight into the underlying mechanisms that bring about the acquired RBC flickering time courses. It is important to note that the analogy on which the model is based in the "Theory of methods" is a gross simplification of the RBC membrane. While we can view only the surface of the RBC using DIC microscopy, it is well established that the RBC membrane is a composite structure consisting of a fluid lipid–protein bilayer and a quasi-two-dimensional spectrin–actin network (Agar and Board 1983). Both components contribute to thickness fluctuations in the cell and this is described in detail by Zilker et al. (1992). Our intention, however, was not to model the viscoelastic properties of the membrane, but to formulate a model that yielded realistic empirical data suitable for testing the various data processing protocols. Indeed, the results obtained from it closely represented those seen in the experiments. Figure 4 shows that the metric (slope of power spectrum) differed between young and old cells because the propagation of waves through the latter was more damped, and so decayed more rapidly. Moreover, it validated the power spectrum line-fitting method.

Conclusions

Previous results (Costa et al. 2008) that showed a demonstrable difference in some features of RBC membrane flickering brought out by signal processing in the old and young populations of RBCs were confirmed. However, a novel approach to the experiments was used here, namely: (1) choosing to monitor the central pixel of an RBC, (2) using DIC microscopy with (3) high-speed imaging, and (4) power-spectral analysis with line fitting. The study was extended by: (1) measuring individual cells upon perturbation of the normal conditions: (a) temperature, (b) ATP concentration, and (c) water diffusion; and (2) developing a computer simulation of the time series acquired from typical young and old RBCs.

The results showed that RBC flickering frequency was resistant to perturbations in temperature. We measured the effect of varying the sample temperature and found an insignificant change in the power spectrum metric. Thermal fluctuations would be expected to show an Arrhenius dependence of the metric on temperature, but this was not the case. On the other hand, when Brownian motion was measured by using rigid latex spheres, there was a strong correlation between the power spectrum metric and the temperature of the system. This is strong evidence that the phenomenon in the RBC is more than thermally driven; other enzymic/cytoskeletal processes which are temperature compensated (i.e., operate in the same way over a wide temperature range such as is found between the core body temperature and the extremities of, say, the fingers) are postulated to be involved in RBC membrane flickering.

Flickering was also resistant to perturbations in ATP concentration, and to changes in viscosity and inhibition of AQP3 by glycerol. One explanation for these results is that the analysis is insensitive to the type of changes in flickering that these perturbations bring about. High variation was seen amongst different time courses recorded from the same cell within a few minutes of each other (this phenomenon was observed in the computer simulations also). The changes in flickering that the perturbations brought about may be too low to overcome this randomness and so may be invisible to the analyses. Our statistical analysis indicated that, at least with the present methods of time series analysis, a cell could not be designated, with a high level of confidence, as old or young based on its flickering metric.

Annotated *Mathematica* programs that perform the analysis of flickering time series are available from the authors.

Acknowledgments P.W. Kuchel thanks the Australian Research Council for a Discovery Project grant. Mr. Justin Wishart is thanked for expert advice on statistical analysis. D. Szekely thanks the University of Sydney for a Postgraduate Award, and T.W. Yau thanks the University of Sydney and ANSTO for a joint Postgraduate Award.

Appendix

This section is presented as a prelude to the analyses of time series that are derived from the well-known Fourier transform.

Fourier transform

The Fourier transform, a linear operator, maps one function of a given independent variable (time) onto another function of a so-called conjugate variable (frequency) (Butz 2006). The Fourier transform decomposes a function into a continuous spectrum of its frequency components, and the inverse transform synthesizes a function from its spectrum of frequency components. Similarly, the discrete Fourier transform maps a time series onto a finite spectrum of its frequency components (Bracewell 1999).

The Fourier transform of a complex-valued Lebesgue-integrable function, $x(t)$ is defined in discrete-series processing as the function

$$X(f) = \int_{-\infty}^{\infty} x(t)\mathrm{e}^{-\mathrm{i}2\pi ft}\mathrm{d}t, \tag{5}$$

for every real number f.

When the independent variable t represents time (with SI unit of seconds), the transform variable f represents ordinary frequency (in Hertz). The complex-valued function, X, is said to represent x in the frequency domain, i.e., if x is a continuous function, then it can be reconstructed from X by the inverse transform

$$x(t) = \int_{-\infty}^{\infty} X(f)\mathrm{e}^{\mathrm{i}2\pi ft}\mathrm{d}f, \tag{6}$$

for every real number t, and premultiplied by a scaling parameter (here, given the arbitrary value 1.0).

The interpretation of X is aided by expressing it in polar coordinate form

$$X(f) = A(f)\mathrm{e}^{-\mathrm{i}\phi(f)}, \tag{7}$$

where

$$A(f) = |X(f)| \tag{8}$$

is the amplitude, and

$$\Phi(f) = \mathrm{Angle}(X(f)) \tag{9}$$

is the phase.

Then the inverse transform can be written

$$x(t) = \int_{-\infty}^{\infty} A(f)\mathrm{e}^{\mathrm{i}(2\pi ft+\phi(f))}\mathrm{d}f, \tag{10}$$

which is a recombination of all the frequency components of $x(t)$. Each component is a sinusoid expressed in complex form, $\mathrm{e}^{\mathrm{i}2\pi ft}$, whose amplitude is $A(f)$ and whose initial phase angle (at $t = 0$) is $\Phi(f)$.

Wavelet transform

It is important in many situations to obtain the temporal structure of the frequency content of a time series in a transparent way. One way to obtain both time and frequency localization is to use a windowed Fourier transform. As the name suggests, the signal is multiplied by a window function $b(t - t_0)$, where $b(t)$ is nonzero only in a finite region at and beyond $t = 0$. Then the Fourier transform of $x(t)$ $b(t - t_0)$, is

$$\hat{X}(f, t_0) = \int_{-\infty}^{\infty} x(t)b(t - t_0)\mathrm{e}^{-\mathrm{i}ft}\mathrm{d}t. \tag{11}$$

This gives the frequency content of the signal near $t = t_0$. It is clear that only the signal around $t = t_0$ contributes to $\hat{X}(f, t_0)$, since this is the part of the signal that is "seen" through the window, while the rest is cut off by the function $b(t)$. As the window is moved along the time axis, different parts of the signal are "seen," this accomplishes the aim of finding a time–frequency description of $f(t)$.

The continuous wavelet transform of a discrete sequence x_n is defined as the convolution of x_n with a scaled and translated version of $\psi_0(t)$, the "mother" wavelet (Torrence and Compo 1998)

$$W_n(s) = \sum_{n'=0}^{N-1} x_{n'}\psi^*\left[\frac{(n' - n)\delta t}{s}\right], \tag{12}$$

where N is the total number of points in the time series; ψ is the mother wavelet scaled by the real factor s and translated along the localized time index n; δt is the time separation between points in the series; and the asterisk denotes the complex conjugate of the respective function. By varying n and s through appropriate ranges, an image is constructed showing both the amplitude of any features versus the wavelet scale.

The choice of the mother wavelet, $\psi_0(t)$, is to some extent arbitrary but the particular choice is very important as it determines the features that are enhanced after its convolution with the data. In the present work, the Morlet wavelet (Goupillaud et al. 1984) was used, whose equation is

$$\pi^{\frac{1}{4}} e^{i\omega_0 t} e^{-\frac{t^2}{2}}. \quad (13)$$

Magnitude-mode processing

Magnitude-mode processing has been used to recover dispersion-mode information from Fourier transforms for applications in ion cyclotron resonance, infrared interferometry, and NMR spectroscopy (Brenna and Yeager 1995; Williams and Marshall 1992). It is calculated using the following equation:

$$m(f) = \sum_{i=1}^{N} \sqrt{\mathrm{Re}(X_i(f))^2 + \mathrm{Im}(X_i(f))^2}, \quad (14)$$

where $m(f)$ is the magnitude-mode spectrum, N is the number of time series acquired, and $\mathrm{Re}(X_i(f))$ and $\mathrm{Im}(X_i(f))$ are the real and imaginary parts of the ith Fourier spectrum, respectively.

Detrended fluctuation analysis

Detrended fluctuation analysis (DFA) (Peng et al. 1995) gives a measure of how fluctuations in a time series differ from the trend obtained from different scales of windows of that time series. Essentially, a time series, $X = \{x_1, x_2, \ldots, x_N\}$ of length N is integrated, as $y(k) = \sum_{i=1}^{k} x_i - X_{\mathrm{ave}}$, where X_{ave} is the mean of X. The integrated time series, $y(k)$, is then divided into windows of equal length, n. A linear trend is found for the data points in that window [let $y_n(k)$ represent the y-coordinate of the straight-line segments], and this is then subtracted from those data points (thereby detrending it). The root mean squares (RMS) of the residuals is calculated by

$$F(n) = \sqrt{\frac{1}{N} \sum_{k=1}^{N} (y(k) - y_n(k))^2}. \quad (15)$$

The computation is repeated over all time scales ("box sizes") to give a relationship between $F(n)$, the average fluctuation as a function of box size, and the box size, n. When fitted to a line, DFA gives a measure of the extent of randomness of a signal. A slope of nonlinear trend represents a time series of uncorrelated randomness; while a linear trend with slope 1.0 indicates red noise; i.e., the time series has long-range correlations and exhibits scale-invariant properties (Fig. 1e).

Multiscale entropy

Multiscale entropy (MSE) (Costa et al. 2002) analysis quantifies the extent of irregularity of a time series over a range of scales. For this method, a moving average of run length, s (the scale), of the time series is taken and sample entropy is calculated using the method outlined in Richman and Moorman (2000). Briefly, consider the time series of length N: $X = \{x_1, x_2, \ldots, x_N\}$. Consider the m-length vector $u_m(i) = \{x_i, x_{i+1}, \ldots, x_N\}$, $1 \le i \le N - m + 1$. Let $n_i^m(r)$ represent the number of vectors $u_m(j)$ that are proximal to the vector $u_m(i)$, i.e., the number of vectors whose Euclidean distance from each other is less than or equal to r, $d[u_m(j), u_m(i)] \le r$. The proximity distance, r, was defined as 15% of the standard deviation of the time series X. The probability that vector $u_m(j)$ is proximal to the vector $u_m(i)$ is

$$C_i^m(r) = \frac{n_i^m(r)}{N - m + 1}. \quad (16)$$

Richman and Moorman (Richman and Moorman 2000) defined the value of the sample entropy as

$$S_E(m, r, N) = -\ln\left(\frac{U^{m+1}(r)}{U^m(r)}\right), \quad (17)$$

where $U^m(r)$ and $U^{m+1}(r)$ are similar to $C^m(r)$ and $C^{m+1}(r)$, except for the special properties which result from the calculation of Shannon's entropy (Shannon 1948), namely: (1) the distance between two vectors is the absolute maximum difference between their components, (2) self-matches are excluded, i.e., vectors are not compared against themselves, and (3) given a particular time series with N data points, only the first $N - m$ vectors of length m, $u_m(i)$ are considered, ensuring that, for $1 \le i \le N - m$, the vector $u_{m+1}(i)$ of length $m + 1$ is also defined. Thus

$$S_E(m, r, N) = -\ln \frac{\sum_{i=1}^{N-m} n_i'^m}{\sum_{i=1}^{N-m} n_i'^{m+1}}, \quad (18)$$

where $n_i'^m$ and $n_i'^{m+1}$ differ from n_i^m and n_i^{m+1} in that self-matches are not considered.

The scale (s) is then iterated and the process repeated over a range of scales. In the case of white noise, maximum entropy occurs at the smallest scale, and decays over subsequent scales. In contrast, red noise represents fluctuation complexity over multiple scales, so the MSE remains relatively constant (Fig. 1f).

References

Agar NS, Board PG (1983) Red blood cells of domestic mammals. Elsevier, Amsterdam

Ballas SK, Flynn JC, Pauline LA, Murphy DL (1986) Erythrocyte Rh-antigens increase with red-cell age. Am J Hematol 23:19–24. doi:10.1002/ajh.2830230104

Benga G, Popescu O, Pop VI, Holmes RP (1986) *p*-(Chloromercuri)benzenesulfonate binding by membrane proteins and the inhibition of water transport in human erythrocytes. Biochemistry 25:1535–1538. doi:10.1021/bi00355a011

Benga G, Chapman BE, Matei HV, Gallagher C, Blyde D, Kuchel PW (2002) Effects of *p*-chloromercuribenzene sulfonate on water transport across the marsupial erythrocyte membrane. J Comp Physiol [B] 172:513–518. doi:10.1007/s00360-002-0277-9

Bennett V, Baines AJ (2001) Spectrin and ankyrin-based pathways: metazoan inventions for integrating cells into tissues. Physiol Rev 81:1353–1392

Bernhardt I, Ellory JC (2003) Red cell membrane transport in health and disease. Springer, Heidelberg

Bessis M (1972) Red cell shapes. An illustrated classification and its rationale. Nouv Rev Fr Hematol 12:721–745

Bhakdi S, Tranumjensen J (1991) Alpha-toxin of *Staphylococcus-aureus*. Microbiol Rev 55:733–751

Blowers R, Clarkson EM, Maizels M (1951) Flicker phenomenon in human erythrocytes. J Physiol 113:228–239

Bracewell R (1999) The Fourier transform and its applications, 3rd edn. McGraw-Hill, New York

Brenna JT, Yeager KE (1995) Direct determination of deuterium in untreated water and urine by NMR: application to DLW analysis. Am J Physiol 268:E1018–E1026

Brochard F, Lennon JF (1975) Frequency spectrum of the flicker phenomenon in erythrocytes. J Phys I 11:1035–1047

Browicz T (1890) Weitere beobachtungen über bewegungsphänomene an roten blutkörperchen in pathologischen zuständen. Centralblatt Med Wiss 28:625

Butz T (2006) Fourier transform for pedestrians. Springer, Heidelberg

Cabot RC (1901) A guide to the clinical examination of the blood. Green & Co., London

Cogswell CJ, Sheppard CJR (1992) Confocal differential interference contrast (DIC) microscopy—including a theoretical-analysis of conventional and confocal DIC imaging. J Microsc Oxford 165:81–101

Conlon T, Outhred R (1972) Water diffusion permeability of erythrocytes using an NMR technique. Biochim Biophys Acta 288:354–361. doi:10.1016/0005-2736(72)90256-8

Costa M, Goldberger AL, Peng CK (2002) Multiscale entropy analysis of complex physiologic time series. Phys Rev Lett 89:068102–068104

Costa M, Ghiran I, Peng CK, Nicholson-Weller A, Goldberger AL (2008) Complex dynamics of human red blood cell flickering: alterations with in vivo aging. Phys Rev E 78:78, 020901

Coza A, Morariu VV (2003) Generating $1/f_{\beta}$ noise with a low-dimensional attractor characteristic: its significance for atomic vibrations in proteins and cognitive data. Physica A 320:449–460. doi:10.1016/S0378-4371(02)01649-7

Einstein A (1905) The motion of elements suspended in static liquids as claimed in the molecular kinetic theory of heat. Ann Phys 17:549–560. doi:10.1002/andp.19053220806

Evans J, Gratzer W, Mohandas N, Parker K, Sleep J (2008) Fluctuations of the red blood cell membrane: relation to mechanical properties and lack of ATP dependence. Biophys J 94:4134–4144. doi:10.1529/biophysj.107.117952

Fricke K, Sackmann E (1984) Variation of frequency spectrum of the erythrocyte flickering caused by aging, osmolarity, temperature and pathological changes. Biochim Biophys Acta 803:145–152. doi:10.1016/0167-4889(84)90004-1

Gallagher PG, Forget BG (1998) Hematologically important mutations: spectrin and ankyrin variants in hereditary spherocytosis. Blood Cells Mol Dis 24:539–543. doi:10.1006/bcmd.1998.0217

Gardiner CW (2004) Handbook of stochastic methods for physics, chemistry and the natural sciences. Springer, Berlin

Garrett RH, Grisham CM (1999) Biochemistry. Harcourt, Florida

Gouaux E (1998) Alpha-haemolysin from *Staphylococcus aureus*: an archetype of beta-barrel, channel-forming toxins. J Struct Biol 121:110–122. doi:10.1006/jsbi.1998.3959

Goupillaud P, Grossman A, Morlet J (1984) Cycle-octave and related transforms in seismic signal analysis. Geoexploration 23:85–102. doi:10.1016/0016-7142(84)90025-5

Gov NS, Safran SA (2005) Red blood cell membrane fluctuations and shape controlled by ATP-induced cytoskeletal defects. Biophys J 88:1859–1874. doi:10.1529/biophysj.104.045328

Hansen PE, Skibsted U, Nissen J, Rae CD, Kuchel PW (2001) ^{1}H NMR of compounds with low water solubility in the presence of erythrocytes: effects of emulsion phase separation. Eur Biophys J 30:69–74. doi:10.1007/s002490000108

Jarvis SM, Young JD (1986) Nucleoside transport in rat erythrocytes—2 components with differences in sensitivity to inhibition by nitrobenzylthioinosine and para-chloromercuriphenyl sulfonate. J Membr Biol 93:1–10. doi:10.1007/BF01871013

Khan A, Gibson JS, Ellory JC (2000) Oxygen-dependent KCl cotransport in ghosts from normal human red blood cells. J Physiol 527:303–318

Kirk K, Raftos JE, Kuchel PW (1986) Triethyl phosphate as an internal ^{31}P NMR reference in biological samples. J Magn Reson 70:484–487

Krol AY, Grinfeldt MG, Levin SV, Smilgavichus AD (1990) Local mechanical oscillations of the cell-surface within the range 0.2–30 Hz. Eur Biophys J 19:93–99. doi:10.1007/BF00185092

Kuchel PW, Benga G (2005) Why does the mammalian red blood cell have aquaporins? Biosystems 82:189–196. doi:10.1016/j.biosystems.2005.07.002

Kuchel PW, Eykyn TR, Regan DG (2004) Measurement of compartment size in *q*-space experiments: Fourier transform of the second derivative. Magn Reson Med 52:907–912. doi:10.1002/mrm.20219

Levin S, Korenstein R (1991) Membrane fluctuations in erythrocytes are linked to MgATP-dependent dynamic assembly of the membrane skeleton. Biophys J 60:733–737. doi:10.1016/S0006-3495(91)82104-X

Lind I, Ahnert-Hilger G, Fuchs G, Gratzl M (1987) Purification of alpha-toxin from *Staphylococcus aureus* and application to cell permeabilization. Anal Biochem 164:84–89. doi:10.1016/0003-2697(87)90371-X

Lovric VA, Archer GT, Wisdom L, Robson J, Raftos J, Coulits N, Ribeiro A, Stewart M, Jindra J, Schuller M (1985) Thirty-five-day modified red cells and 7-day stored platelet concentrates from triple bags of identical PVC formulation. Vox Sang 49:181–186. doi:10.1111/j.1423-0410.1985.tb00791.x

Miller DM (1963) "Flickering" in protoplasts of *Bacillus megaterium*. Science 139:1060–1061. doi:10.1126/science.139.3559.1060

Milotti E (1995) Linear-processes that produce 1/f or flicker noise. Phys Rev E Stat Phys Plasmas Fluids Relat Interdiscip Topics 51:3087–3103. doi:10.1103/PhysRevE.51.3087

Mittelman L, Levin S, Korenstein R (1991) Fast cell-membrane displacements in lymphocytes-b—modulation by dihydrocytochalasin-b and colchicine. FEBS Lett 293:207–210. doi:10.1016/0014-5793(91)81188-E

Mittelman L, Levin S, Verschueren H, Debaetselier P, Korenstein R (1994) Direct correlation between cell-membrane fluctuations, cell filterability and the metastatic potential of lymphoid-cell lines. Biochem Biophys Res Commun 203:899–906. doi:10.1006/bbrc.1994.2267

Morariu VV, Buimaga-Iarinca L, Vamos C, Soltuz SM (2007) Detrended fluctuation analysis of autoregressive processes. Fluct Noise Lett 7:L249–L255. doi:10.1142/S0219477507003908

Pages G, Szekely D, Kuchel PW (2008) Erythrocyte-shape evolution recorded with fast-measurement NMR diffusion-diffraction. J Magn Reson Imaging 28:1409–1416. doi:10.1002/jmri.21588

Peng CK, Buldyrev SV, Goldberger AL, Havlin S, Mantegna RN, Simons M, Stanley HE (1995) Statistical properties of DNA-

sequences. Physica A 221:180–192. doi:10.1016/0378-4371(95)00247-5

Pulvertaft RJV (1949) Vibratory movement in the cytoplasm of erythrocytes. J Clin Pathol 2:281–283. doi:10.1136/jcp.2.4.281

Richman JS, Moorman JR (2000) Physiological time-series analysis using approximate entropy and sample entropy. Am J Physiol Heart Circ Physiol 278:H2039–H2049

Roudier N, Verbavatz JM, Maurel C, Ripoche P, Tacnet F (1998) Evidence for the presence of aquaporin-3 in human red blood cells. J Biol Chem 273:8407–8412. doi:10.1074/jbc.273.14.8407

Shaka AJ, Keeler J, Freeman R (1983) Evaluation of a new broadband decoupling sequence—WALTZ-16. J Magn Reson 53:313–340

Shannon CE (1948) A mathematical theory of communication. AT&T Tech J 27:623–656

Stewart GW, Ellory JC, Klein RA (1980) Increased human red-cell cation passive permeability below 12°C. Nature 286:403–404. doi:10.1038/286403a0

Strey H, Peterson M, Sackmann E (1995) Measurement of erythrocyte membrane elasticity by flicker eigenmode decomposition. Biophys J 69:478–488. doi:10.1016/S0006-3495(95)79921-0

Torrence C, Compo GP (1998) A practical guide to wavelet analysis. Bull Am Meteotol Soc 79:61–78. doi:10.1175/1520-0477(1998)079<0061:APGTWA>2.0.CO;2

Tuvia S, Levin S, Bitler A, Korenstein R (1998) Mechanical fluctuations of the membrane-skeleton are dependent on f-actin atpase in human erythrocytes. J Cell Biol 141:1551–1561. doi:10.1083/jcb.141.7.1551

Waugh RE, Narla M, Jackson CW, Mueller TJ, Suzuki T, Dale GL (1992) Rheologic properties of senescent erythrocytes—loss of surface-area and volume with red-blood-cell age. Blood 79:1351–1358

Williams CP, Marshall AG (1992) Hartley/Hilbert transform spectroscopy: absorption-mode resolution with magnitude-mode precision. Anal Chem 64:916–923. doi:10.1021/ac00032a016

Wolfram S (1983) Statistical-mechanics of cellular automata. Rev Mod Phys 55:601–644. doi:10.1103/RevModPhys.55.601

Wolfram S (2007) The *Mathematica* book. Wolfram Research Inc., Champaign

Yang BX, Ma TH, Verkman KS (2001) Erythrocyte water permeability and renal function in double knockout mice lacking Aquaporin-1 and Aquaporin-3. J Biol Chem 276:624–628. doi:10.1074/jbc.M008664200

Zilker A, Ziegler M, Sackmann E (1992) Spectral analysis of erythrocyte flickering in the 0.3–4 μ^{-1} regime by microinterferometry combined with fast image processing. Phys Rev A 46:7998–8001. doi:10.1103/PhysRevA.46.7998